Supplemental Materials

Molecular Biology of the Cell

Goupil et al.

SUPPLEMENTAL MATERIAL – Goupil, Amini *et. al.*

Movie S1. The P_4 blastomere does not complete cellular abscission. Related to Figure 1A. Time-lapse movie of a control embryo expressing NMY-2::GFP (green), a membrane marker (TagRFP::PH, magenta) and a germ granule marker (PGL-1::RFP, magenta). Z stacks (0.5 µm each) were acquired every 35 s and a maximum intensity projection of 3 consecutive stacks is shown for each frame. In somatic cells (lacking PGL-1::RFP signal), the NMY-2-positive midbody ring that forms after cytokinesis is released and degraded within minutes but remains stably present at the interstitial membrane separating the two PGCs (PGL-1::RFP-positive cells). Playback rate is 140x real time (four frames/second). Anterior is to the left. Scale bar, 10 µm.

Movie S2. P_4 division into Z_2 and Z_3 in control or ANI-2-depleted embryos. Related to Figure 3B. Time-lapse movies of control (left) and *ani-2*(RNAi) (right) embryos expressing a membrane marker (mNG::PH, green) and a nucleus marker (mCherry::H2B, magenta). Z stacks (0.75 µm each) were acquired every 180 s and a maximum intensity projection of 2 consecutive stacks is shown for each frame. The membrane between Z_2 and Z_3 is stable in control embryos but collapses during rotation in ANI-2-depleted embryos. Playback rate is 720x real time (four frames/second). Anterior is to the left. Scale bar, 10 µm.

Table S1. Strains used in this study

Strain	Genotype
N2	Wild type
UM227	*unc-119(ed3) III; ltIs38[pAA1; Ppie-1::GFP::PH(PLC1delta1); unc-119(+)] III*
UM456	*cpSi20[Pmex-5::TAGRFPT::PH::tbb-2 3'UTR; unc-119 (+)] I; unc-119(ed3) III; ltIs86[pASM65; Ppie-1::ANI-1(fl cDNA)::GFP; unc-119(+)]; zuIs244[Pnmy-2::PGL-1::mRFP-1; unc-119(+)]*
UM458	*cp13[NMY-2::GFP + LoxP]) I; cpSi20[Pmex-5::TAGRFPT::PH::tbb-2 3'UTR; unc-119(+)] I; unc-119(ed3) III; zuIs244[Pnmy-2::PGL-1::mRFP-1; unc-119(+)]*
UM463	*cpIs42[Pmex-5::mNeonGreen::PLCδ-PH::tbb-2 3'UTR; unc-119(+)] II; ltIs37[pAA64; Ppie-1::mCherry::HIS-58; unc-119(+)] IV*
UM477	*unc-119(ed3) III; ltIs38[pAA1; Ppie-1::GFP::PH(PLC1delta1); unc-119(+)] III; zen-4(or153ts) IV*
UM480	*nmy-2(ne3409) I; unc-119(ed3) III; ltIs38[pAA1; Ppie-1::GFP::PH(PLC1delta1); unc-119(+)] III*
UM502	*cpSi20[Pmex-5::TAGRFPT::PH::tbb-2 3'UTR; unc-119 (+)] I; unc-119(ed3) III; zuIs244[Pnmy-2::PGL-1::mRFP; unc-119(+)]; ltIs20 [pASM10; Ppie-1::GFP::unc-59; unc-119(+)];*
UM608	*cpSi20[Pmex-5::TAGRFPT::PH::tbb-2 3'UTR; unc-119(+)] I; unc-119(ed3) III; zuIs244[Pnmy-2::PGL-1::mRFP; unc-119(+)]; ltIs154[pOD539(pBG3); Ppie-1::C08C3.4::GFP; unc-119(+)]*
OD182	*unc-119(ed3) III; ltIs28[pASM14; Ppie-1/GFP-TEV-Stag::ANI-1; unc-119(+)]; ltIs44[pAA173; Ppie-1/mCherry::PH(PLC1delta1); unc-119(+)]*
OD183	*unc-119(ed3) III; zuIs45[Pnmy-2::NMY-2::GFP; unc-119(+)] V; ltIs44[pAA173; Ppie-1::mCherry::PH(PLC1delta1); unc-119(+)]*
OD239	*cyk-4(or749ts) III; ltIs38[pAA1; Ppie-1/GFP::(PLC1delta1); unc-119(+)] III; ltIs37[pAA64; Ppie-1::mCherry::his-58; unc-119(+)] IV*
OD449	*unc-119(ed3) III; ltIs44[pAA173; Ppie-1::mCherry::PH(PLC1 delta 1); unc-119(+)]; ltIs154[pOD539(pBG3); Ppie-1::C08C3.4::GFP; unc-119(+)]*
JCC146	*cyk-1(or596ts) III; unc-119(ed3)III; ltIs38[pAA1; Ppie-1::GFP::(PLC1delta1); unc-119(+)] III; ltIs37[pAA64; Ppie-1::mCherry::his-58; unc-119(+)] IV*
MG685	*mgSi43[Pcyk-4::cyk-4::GFP::pie-1 3'UTR; unc-119(+)] II; unc-119(ed3) III*

Table S2. Genes depleted by RNAi.

C. elegans gene name and designation		Mammalian homologue	Phenotypic class[1]	RNAi treatment time (hrs)[2]	RNAi clone designation
ani-2	K10B2.5	Anillin	F2	24-72	sjj_K10B2.5
ani-1	Y49E10.19	Anillin	n/a	24	sjj_Y49E10.19
cyk-7	C08C3.4	?	F2	48	sjj_C08C3.4
cyk-4	K08E3.6	MgcRacGAP/ RacGAP50	F3	6	sjj_K08E3.6
zen-4	M03D4.1	MKLP1	n/a	8	sjj_M03D4.1
rho-1	Y51H4A.3	Rho	F3	24	cenix:169-h12
let-502	C10H11.9	ROCK	F2	24	sjj_C10H11.9
ect-2	T19E10.1a	Ect2	F2	8	sjj_T19E10.1a
unc-59	W09C5.2	Septin	n/a	24	sjj_W09C5.2
cyk-1	F11H8.4	Formin	n/a	24	sjj_F11H8.4
nmy-2	F20G4.3	Non-muscle myosin II	F3	24	sjj_F20G4.3
act-4	M03F4.2	Actin	F3	18-24	sjj_M03F4.2
unc-45	F30H5.1	Unc45a, Unc45b	F2	24	sjj_F30H5.1
hmgs-1	F25B4.6	HMGCS2	F4	48	sjj_F25B4.6
hmgr-1	F08F8.2	HMGCR	F4	48	sjj_F08F8.2
ostd-1	M01A10.3	RPN2	F2	48	sjj_M01A10.3
ptc-1	ZK675.1	Patched	n/a	24	cenix:233-g12
ptc-2	F21H12.4	Patched-like	F1	18	cenix:204-g6
egg-6	K07A12.2	?	F1	18	sjj_K07A12.2
oma-1	C09G9.6	?	F2	24	sjj_C09G9.6
npp-20	Y77E11A.13	SEC13	F1	18	sjj_Y77E11A.13
?	F30B5.4	OSGIN1/2	F3	48	sjj_F30B5.4
?	Y32G9B.1	?	F2	48	sjj_Y32G9B.1

[1]From Phenobank Database (http://www.worm.mpi-cbg.de/phenobank/cgi-bin/MenuPage.py) and (Green *et al.*, 2011).

[2]RNAi feeding treatments for less than 24 hrs were started at the adult stage, for more than 24 hrs were started at the L4 larval stage.

SUPPLEMENTAL FIGURE LEGENDS

Figure S1. Quantification of the timing of completion of furrow ingression and midbody ring release. Related to Figures 1 and 2.

(A, D) Schematic depiction of the method used to measure the diameter of the contractile ring over time (A) or the timing of midbody ring release (D). Fluorescence distribution was measured along a line (dotted) drawn on the division plane of somatic and P_4 cells (A) or perpendicular to the interstitial membrane between somatic or germ cell sibling pairs (D). (B, C, E, F) Distribution of NMY-2::GFP (green) and membrane (magenta) signal in somatic (B, E) and Z_2/Z_3 (C, F) blastomeres undergoing contractile ring ingression (B, C) or midbody ring release (E, F). Left panels show representative images and right panels show fluorescence intensities along a line drawn as in (A, D). Green arrows point to peaks of NMY-2::GFP intensities and magenta arrows point to membrane signals. (B, C) The diameter of the contractile ring was assessed by measuring the distance between two maximum peaks at each time point. Furrow ingression was considered as complete when only one peak of NMY-2::GFP was detected (bottom panels). (E, F) The midbody ring position was determined by measuring the distance between the NMY-2::GFP and membrane fluorescence peaks, and midbody ring was considered as "released" when the distance reached 0.4 μm. While all somatic cells attained this stage, no peak separation was observed in PGCs (bottom panels).

Figure S2. Localization of ANI-2 at the PGCs cytoplasmic bridge mirrors that of NMY-2 and CYK-7. Related to Figures 2 and 5.

(A, C, E) Confocal images (maximum intensity projections of 2-3 Z stacks) of PGCs in embryos expressing either CYK-7::GFP (A, C) or NMY-2::GFP (E), from P_4 division to the stage when Z_2 and Z_3 have completed 90º rotation. The localization of ANI-2 at the stable cytoplasmic bridge in fixed samples (C, E) mirrors that of CYK-7::GFP in live samples (A). All scale bars represent 10 μm. (B) Volume (left y-axis) and sum intensity (right y-axis) quantification of CYK-7::GFP as a function of time or different RNAi treatment in live embryos (n=7-10). Error bars represent SEM. (D, F) Volume quantification of

CYK-7::GFP (D) or NMY-2::GFP (F) as a function of number of nuclei in fixed immunostained samples. Linear regressions (full red lines) and confidence intervals (dashed red line) are shown above each data sets.

Figure S3. Several gene depletions have no effect on PGC cytoplasmic bridge stability. Related to Figures 4 and 5. (A) Percentage of embryonic viability after RNAi depletion of several genes used in this study. Time 0 corresponds to the transfer of an animal to an RNAi-inducing condition. *cdk-1* was used as a positive control for embryonic viability. (B) Mid-section confocal time-lapse images of PGCs from embryos expressing membrane (mNG::PH, green) and histone (mCherry::H2B, magenta) markers. Animals were depleted of contractility regulators by RNAi (see Table S2) and stability of the PGC cytoplasmic bridge was assessed by monitoring membrane signal. Scale bar, 10 µm. None of these depletions impacted PGC cytoplasmic bridge stability but induced cytokinetic defects in somatic cells to a varying degree (bottom panels). (C) Schematic representation of ANI-2 localization and depiction of the method used to measure the ANI-2 focus volume at the cytoplasmic bridge between the two PGCs. The 3D rendering of the original ANI-2 fluorescence signal obtained by immunofluorescence (green) and the reconstruction of the focus using Imaris (green) with the germ granules (grey) are shown (see Methods for details). (D) Quantification of the ANI-2 focus volume (dark grey, left axis) at the PGC cytoplasmic bridge as a function of number of nuclei in control embryos. Linear regression (full red line) and confidence interval (dashed red line) are shown above the data set. (E) Confocal images (maximum intensity projections of 5-7 consecutive Z planes) of PGCs in 150-250-cell stage embryos, fixed and stained with antibodies against ANI-2 (green), germ granules (magenta) and DAPI (blue). (F) Quantification of the focus volume of ANI-2 at the PGC cytoplasmic bridge in embryos depleted of the indicated genes by RNAi (E). The red bars represent average ± SD. *$p<0.05$, **$p<0.01$, ***$p<0.001$, n.s. = $p>0.05$. (G) Re-analysis of the data shown in Figure 5B and reporting on the focus volume of ANI-2 at the PGC cytoplasmic bridge, but binned into fragmented and non-

fragmented foci. Focus fragmentation had no effect on the measured volume of the ANI-2 focus. Scale bars, 10 μm.

Figure S4. The accumulation of CYK-4::GFP at the stable PGC cytoplasmic bridge does not depend on several contractility regulators. Related to Figure 6.

(A) Confocal images (maximum intensity projections of 5-7 consecutive Z planes) of PGCs in embryos at the 150-250-cell stage expressing either CYK-4::GFP and fixed and stained with antibodies against GFP (green), ANI-2 (magenta), germ granules (white) and DAPI (blue). Embryos were depleted of the genes indicated by RNAi. Colocalized pixels between the magenta and green channels are shown on the right (white). Scale bar, 10 μm. (B, C) Quantification of the focus volume of CYK-4::GFP (B) or ANI-2 (C) at the PGC cytoplasmic bridge in embryos depleted of the indicated genes by RNAi. The red bars represent average ± SD. *$p<0.05$, **$p<0.01$, ***$p<0.001$, n.s. = $p>0.05$.

Goupil, Amini *et al*. Figure S1

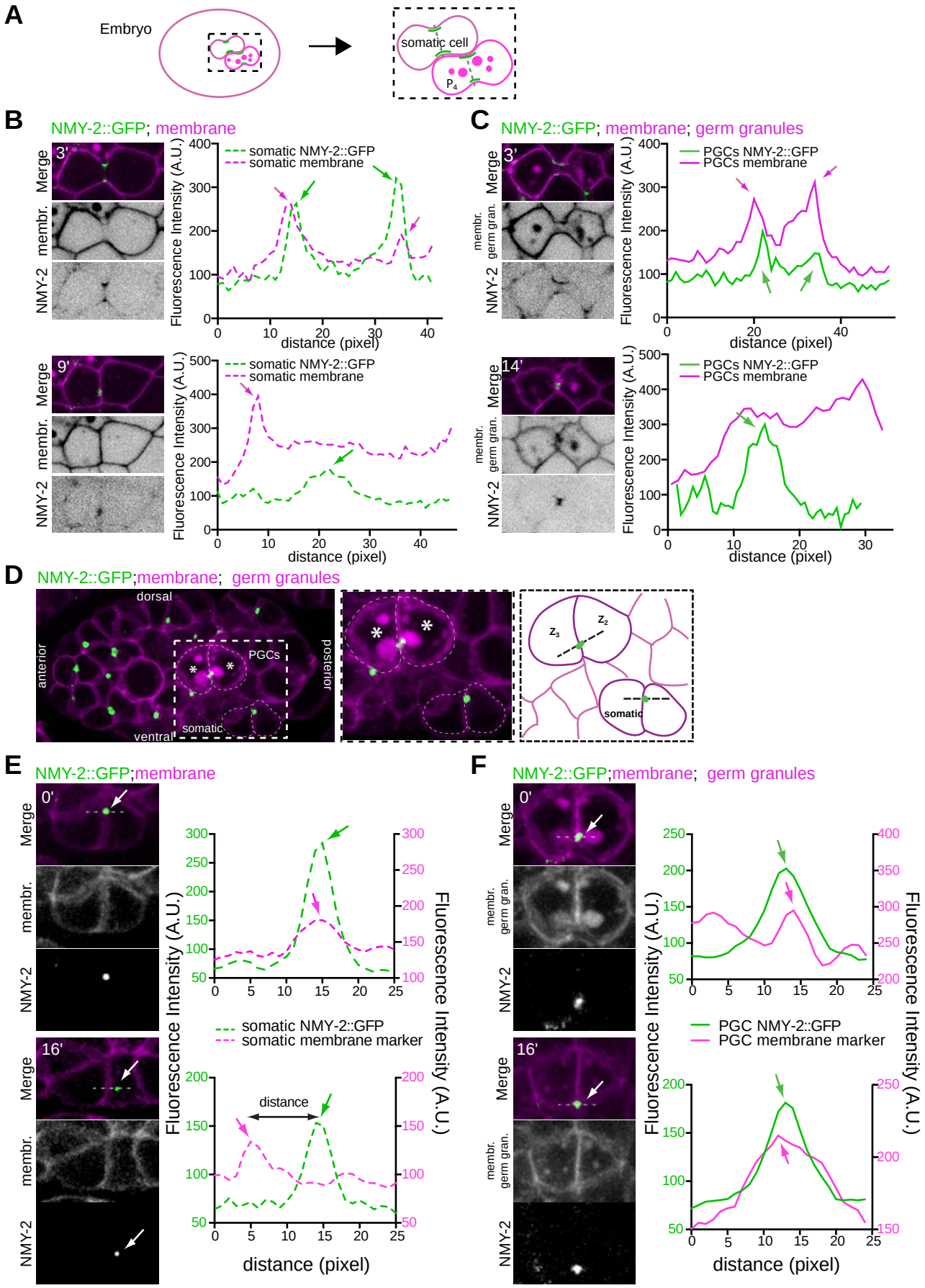

Goupil, Amini *et al.* Figure S2

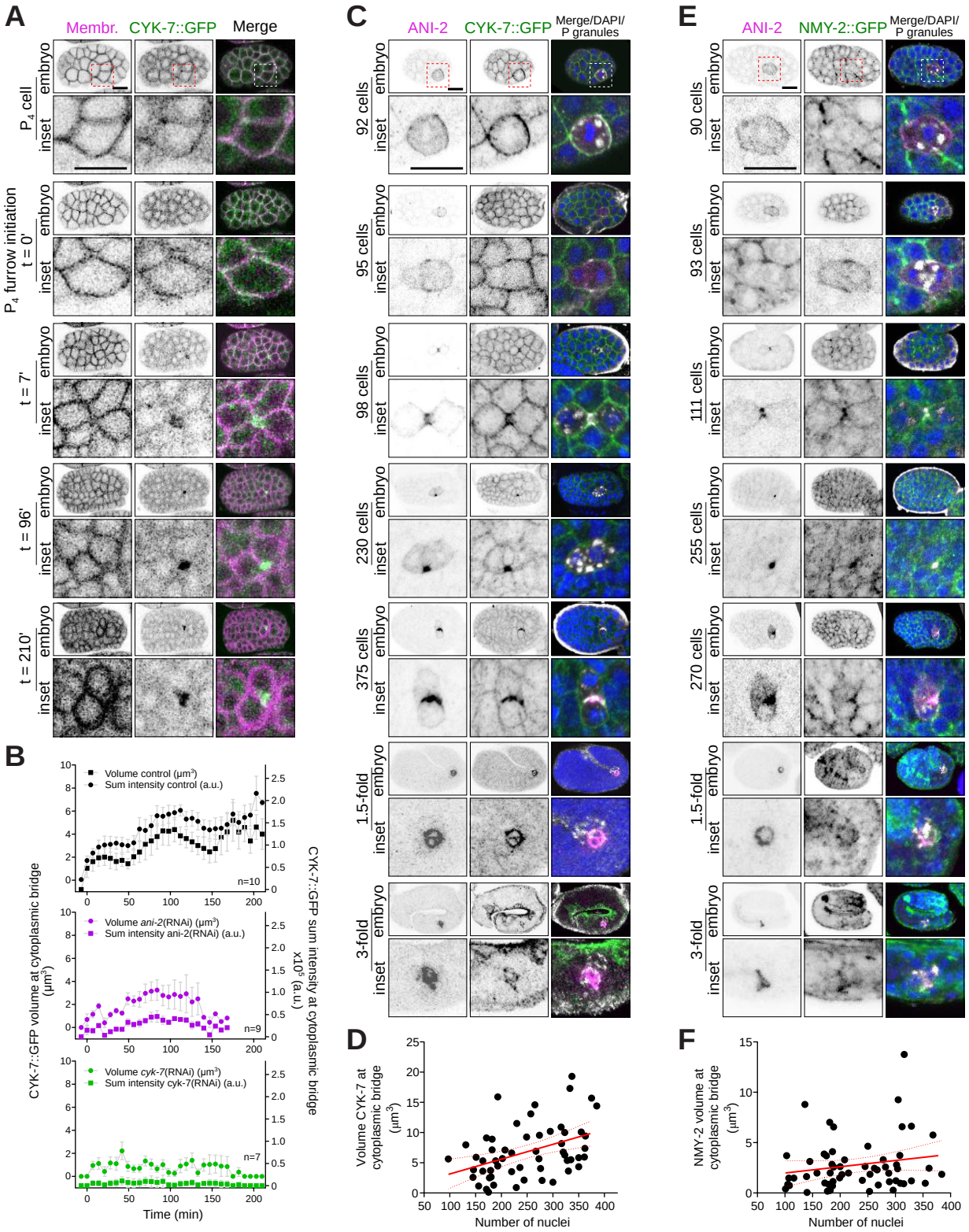

Goupil, Amini *et al*. Figure S3

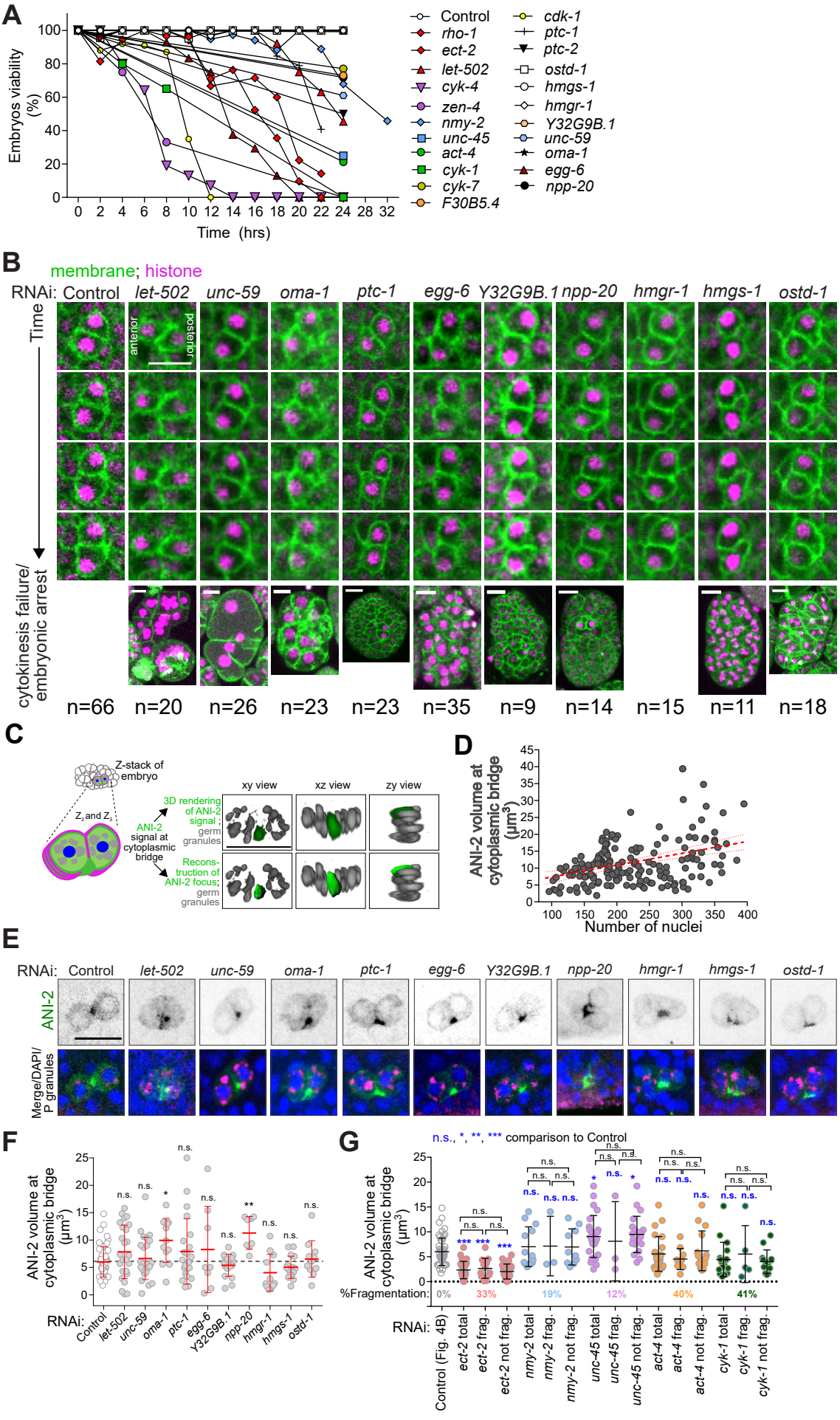

Goupil, Amini *et al.* Figure S4